Cross sections, analyzing powers, and spin-rotation-depolarization observables for 500 MeV proton elastic scattering from ^{12}C and ^{13}C

G. W. Hoffmann, M. L. Barlett,* D. Ciskowski, G. Pauletta,[†] M. Purcell, and L. Ray
Department of Physics, University of Texas, Austin, Texas 78712

J. F. Amann, J. J. Jarmer, K. W. Jones, S. Penttilä, and N. Tanaka
Los Alamos National Laboratory, Los Alamos, New Mexico 87545

M. M. Gazzaly
Department of Physics, University of Minnesota, Minneapolis, Minnesota 55455

J. R. Comfort
Department of Physics, Arizona State University, Tempe, Arizona 85287

B. C. Clark and S. Hama
Department of Physics, The Ohio State University, Columbus, Ohio 43210
(Received 22 November 1989)

New differential cross section ($d\sigma/d\Omega$), analyzing power (A_y), and spin-rotation-depolarization (D_{ij}) data for 500 MeV $\vec{p}+{}^{12}$C,^{13}C elastic scattering are reported. The $d\sigma/d\Omega$ and A_y data span scattering angles from approximately 5°–37° c.m., while the D_{ij} data cover 5°–26° c.m. Except at the largest angles, statistical errors are typically ±1% for $d\sigma/d\Omega$, ±(0.01–0.02) for A_y, and ±(0.03–0.05) for the D_{ij} observables. The data are compared to predictions of Dirac phenomenology and the relativistic-impulse-approximation–Dirac-equation model.

For more than a decade, experiments with proton beams have provided a variety of data that have been used to test models of the nucleon plus nucleus elastic-scattering process at intermediate energies.[1–13] Analyzing powers (A_y) and spin-rotation-depolarization observables (D_{ij}) measured with polarized beams have been particularly useful in guiding theoretical development.[1–13] Even today, the study of spin dependence in the scattering process continues to be an important part of medium energy nuclear physics research. Indeed, during the last few years much work has gone into development of polarized nuclear targets ($A\geq 2$) for use in scattering experiments.[14–16] The intent is clearly to introduce a new degree of freedom, that of target polarization, into the scattering problem. For example, the first phase of one such experiment,[17] $\vec{p}+{}^{13}\vec{\mathrm{C}}$ elastic scattering at 500 MeV, will provide A_{000N} and A_{00NN} data (see Ref. 18 for definition of these observables). Before performing this polarized target experiment we measured differential cross sections ($d\sigma/d\Omega$), analyzing powers, spin-rotation observables D_{SS} and D_{SL}, and the spin-depolarization parameter D_{NN}, for 500-MeV polarized proton elastic scattering from ^{12}C and ^{13}C. These new data, along with a comparison with theoretical results, are reported here.

A complete set of $\vec{p}+{}^{12}$C elastic scattering measurements is intrinsically interesting. Such data provide a means for testing certain aspects of relativistic[19,20] and nonrelativistic models[21] of the scattering process, as well as for studying medium effects, nuclear structure models, and multistep processes.[13] They also allow empirical determination of important components of the nucleon-nucleon (NN) effective interaction.[22] Similar comments apply for $\vec{p}+{}^{13}$C. The $\vec{p}+{}^{13}$C $d\sigma/d\Omega$ and A_y data will also serve as benchmarks for the more difficult $\vec{p}+{}^{13}\vec{\mathrm{C}}$ experiment.

In addition, the $\vec{p}+{}^{12}$C, ^{13}C data are needed for the theoretical interpretation of the $\vec{p}+{}^{13}\vec{\mathrm{C}}$ data. The $\vec{p}+{}^{12}$C data enable determination of phenomenological representations of the twelve nucleon "core" scattering amplitudes and distorted waves that are required in distorted wave Born approximation (DWBA) calculations for $\vec{p}+{}^{13}\vec{\mathrm{C}}$ elastic scattering.[18] The measured ratio of the ^{13}C to ^{12}C differential cross sections can be used to constrain models of the ^{13}C valence neutron wave function. Finally, studies of D_{NN} focus attention on important $\Delta J=1$ contributions to the $\vec{p}+{}^{13}$C elastic scattering amplitude. When these transitions occur D_{NN} becomes less than unity, and the spin-flip probability, given by $\frac{1}{2}(1-D_{NN})$, is nonzero.

The data were taken at the Los Alamos Clinton P. Anderson Meson Physics Facility (LAMPF) with the high resolution spectrometer (HRS) and its focal plane polarimeter (FPP). Experimental details are essentially the same as those discussed elsewhere.[1,2,4–12] The targets were isotopically enriched foils (≥99.9% for ^{12}C and 78–98% for ^{13}C) of known thicknesses ranging from 45–160 mg/cm^2 (±1–2% uncertainty). The beam energy was 494±1 MeV and the overall experimental energy resolution was typically ≤100 keV full width at half maximum (FWHM) for the thin targets. The absolute

 ©1990 The American Physical Society

scale of scattering angle was determined to ±0.1°. The absolute scale for the differential cross sections was determined to within ±10% by normalizing to some ^{12}C cross-section data taken (but unpublished) in an earlier experiment.[7] The relative normalization differences between the ^{12}C and ^{13}C differential cross sections are less than ±3%. The beam polarization was typically 80% and was monitored continuously with a beam line polarimeter. Except at the largest angles, statistical errors are typically ±1% for $d\sigma/d\Omega$, ±(0.01–0.02) for A_y, and ±(0.03–0.05) for D_{ij}. For the $d\sigma/d\Omega$ and A_y data the systematic errors are small ($\leq \pm 2\%$); for the D_{ij} data, the systematic uncertainties in D_{SL} and D_{SS} are $\leq \pm 0.02$, while those for D_{NN} are $\leq \pm 0.04$.

The data[23] (and curves to be discussed) are shown in Figs. 1–3. The ^{13}C/^{12}C differential cross-section ratios versus momentum transfer are plotted in Fig. 4, along with curves to be discussed. The observables for ^{12}C and ^{13}C are similar as expected.

We now discuss results of two types of theoretical calculations. The first is the relativistic-impulse-approximation (RIA)–Dirac-equation model of Ref. 20 for ^{12}C and the relativistic DWBA model of Ref. 18 for ^{13}C. The second is a Dirac optical-model fit[24] to the $\vec{p}+{}^{12}$C data and a $\vec{p}+{}^{13}$C relativistic DWBA calculation that uses the scattering amplitudes and distorted waves from the optical-model fit. The former calculations are fully microscopic, whereas the latter treat only the valence neutron contribution in ^{13}C microscopically.

The first set of calculations for $p+{}^{12}$C based on the RIA-Dirac-equation approach includes the following ingredients: (1) Lorentz invariant amplitudes generated from the SP82 *NN* phase shifts,[20,25] (2) the proton vector density obtained from the ^{12}C charge density,[26] (3) the neutron vector density parametrized as in Eqs. (20) and (21) of Ref. 18 with the surface geometry adjusted to fit the $\vec{p}+{}^{12}$C differential cross-section data (parameter values are given in Ref. 18), and (4) scalar densities obtained from relativistic mean-field theory (RMFT) (Ref. 27) according to Eq. (22) in Ref. 18. The predictions (dashed curves in Fig. 1) qualitatively describe the $\vec{p}+{}^{12}$C data. The corresponding relativistic DWBA predictions for $\vec{p}+{}^{13}$C (from Ref. 18) are shown as dashed curves in Fig. 2. These calculations use the preceding $p+{}^{12}$C RIA-Dirac-equation scattering amplitudes and relativistic distorted waves, a $1p_{1/2}$ single-particle eigenstate from

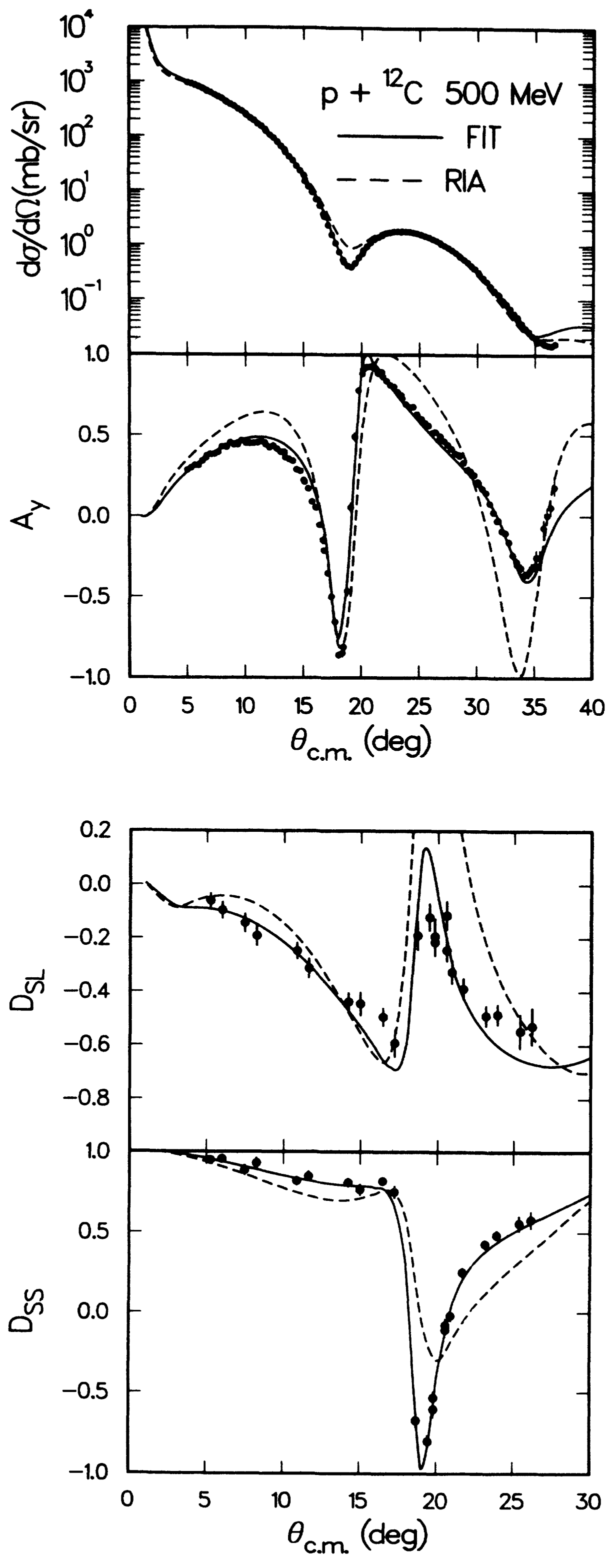

FIG. 1. Elastic differential cross section, analyzing power, and spin-rotation data, and results of calculations, for 500 MeV $\vec{p}+{}^{12}$C. The solid and dashed curves are Dirac optical-model fits and RIA-Dirac-equation model predictions, respectively, as discussed in the text. The errors in the data include statistical uncertainties only.

TABLE I. Best fit Woods-Saxon Dirac optical potentials for 500 MeV $\vec{p}+{}^{12}$C elastic scattering. Each term is of the form $V/[1+\exp((r-r_0A^{1/3})/z)]$ where A is the baryon number of the target.

Potential term	V (MeV)	r_0 (fm)	z (fm)
Real vector	214.05	0.9834	0.4817
Imag vector	−62.63	1.0829	0.4355
Real scalar	−297.11	0.9809	0.5143
Imag scalar	35.23	1.1834	0.3263

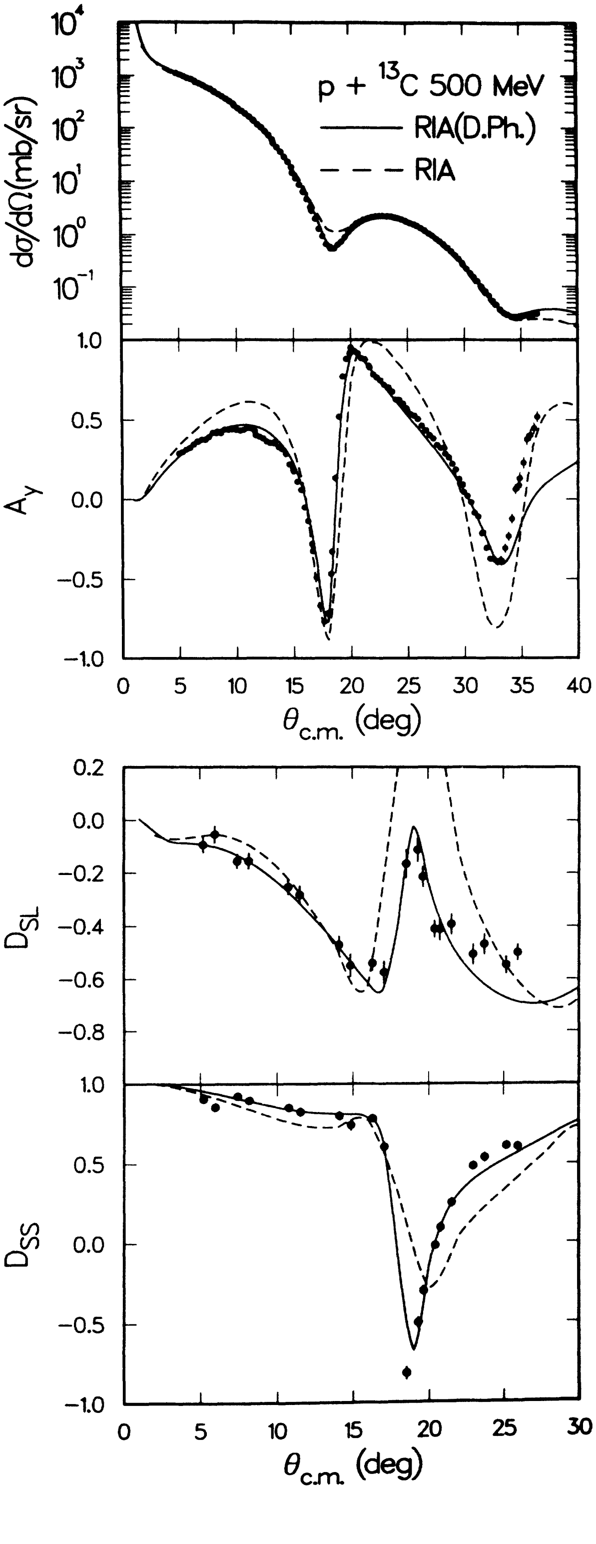

FIG. 2. Elastic differential cross section, analyzing power, and spin-rotation data, and results of calculations, for 500 MeV $\vec{p}+{}^{13}C$. The solid and dashed curves are relativistic DWBA results based on Dirac phenomenology and the RIA optical potentials for ^{12}C, respectively, that were used to compute the twelve nucleon core scattering amplitude and relativistic distorted waves as discussed in the text. The errors in the data include statistical uncertainties only.

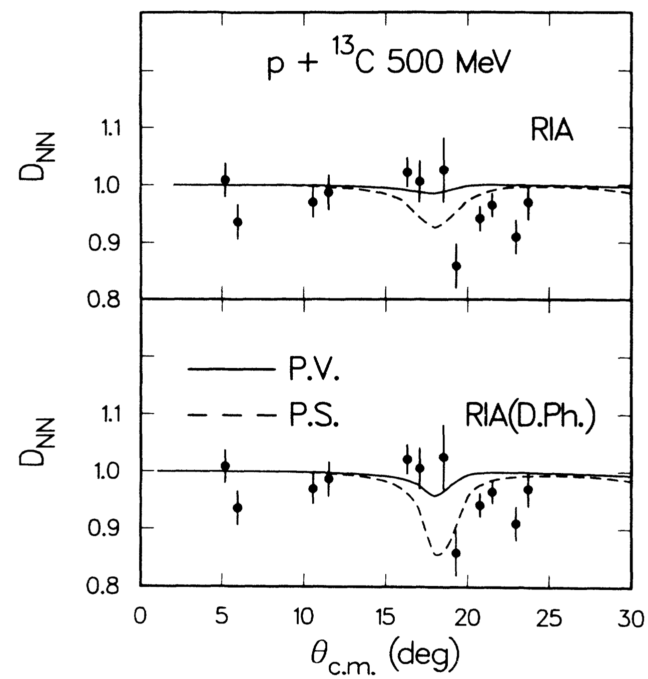

FIG. 3. Data and RIA results for the spin-depolarization observable D_{NN} for 500 MeV $\vec{p}+{}^{13}C$ elastic scattering. The solid and dashed curves are the relativistic DWBA results when the pseudovector and pseudoscalar forms for the Lorentz invariant NN amplitude (Ref. 18) are used, respectively. The curves in the upper (lower) half of the figure correspond to use of the RIA (Dirac phenomenological) ^{12}C optical potential to compute the core scattering amplitudes and distorted waves. The errors in the data include statistical uncertainties only.

ing potentials,[27] and the pseudoscalar form of the NN invariant amplitude.[18] This calculation, referred to as the standard RIA-DWBA, also provides a qualitative fit to the data.

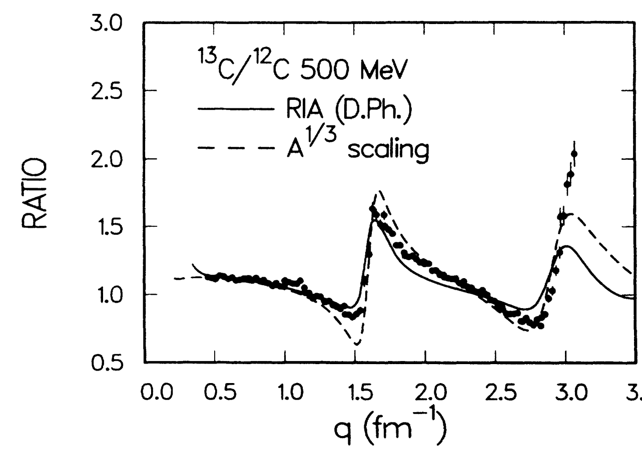

FIG. 4. Ratio of ^{13}C to ^{12}C elastic differential cross sections as a function of momentum transfer. The errors in the data include statistical uncertainties only. The solid and dashed curves are relativistic DWBA and Dirac optical-model results, respectively, as discussed in the text.

For the second set of calculations complex, phenomenological scalar and timelike vector potentials in the Dirac equation[24] were searched to obtain a best fit to the $d\sigma/d\Omega$, A_y, and D_{SL} data for $\vec{p}+{}^{12}C$. The best fit Woods-Saxon parameters are given in Table I; the good fit to the data is shown by the solid curves in Fig. 1. The $\vec{p}+{}^{12}C$ scattering amplitudes and relativistic distorted wave functions from this phenomenological optical model result were then used for the $\vec{p}+{}^{13}C$ relativistic DWBA calculation. Otherwise this $\vec{p}+{}^{13}C$ calculation was the same as that described in the preceding paragraph. The result, indicated by the solid curves in Fig. 2, quantitatively fits the data. The improvement over the standard RIA-DWBA prediction is a direct consequence of using a phenomenological model that accurately reproduces the $\vec{p}+{}^{12}C$ data.

To observe effects due to the 13th nucleon, with proton elastic scattering from an unpolarized ${}^{13}C$ target, the quantity D_{NN} and the small differences between the ${}^{13}C$ and ${}^{12}C$ observables, must be studied. The amount by which D_{NN} differs from unity is determined by a few of the $\Delta J=1$ components of the NN effective interaction[18] along with the valence nucleon wave function. The ${}^{13}C/{}^{12}C$ cross-section ratio primarily depends upon the $\Delta J=0$ components of the NN amplitudes[18] and is particularly sensitive to the large, upper component of the valence nucleon wave function.

In Fig. 16 of Ref. 18, a variety of RIA-DWBA D_{NN} predictions are shown for 500 MeV $\vec{p}+{}^{13}C$. Two of these are compared with the new data in the upper half of Fig. 3; the standard RIA-DWBA result is indicated by the dashed curve; the solid curve also represents a RIA-DWBA result, except that the pseudovector form of the NN invariant amplitude was used, and the isoscalar three-vector current was suppressed.[18] The two curves shown in the lower half of the figure correspond to those in the upper half, except that the phenomenological ${}^{12}C$ distorted waves and scattering amplitudes were used instead. None of the four results fit the data very well. The calculated minimum in D_{NN} at 18° c.m. is constrained by the deep, first minimum in the differential cross section. The suggested sharp minimum at 19° c.m. in the D_{NN} data is hard to fit simultaneously with that of the $d\sigma/d\Omega$.

In Fig. 4, the ${}^{13}C/{}^{12}C$ $d\sigma/d\Omega$ ratio is compared with two model predictions. The ratio, (${}^{13}C$ relativistic DWBA $d\sigma/d\Omega$ using phenomenological distorted waves and core amplitudes)/(the Dirac phenomenological ${}^{12}C$ $d\sigma/d\Omega$) is indicated by the solid line. The dashed curve results from using the Dirac optical potential of Table I to calculate both the ${}^{12}C$ and ${}^{13}C$ cross sections, where in both cases the radii were scaled by $A^{1/3}$ (see Table I). The majority of the structure in the ${}^{13}C/{}^{12}C$ ratio results from the overall $A^{1/3}$ scaling of the nuclear size. The amount of sensitivity to different forms for the ${}^{13}C$-${}^{12}C$ nuclear structure difference is indicated by the small differences among the two curves and the data.

In summary, new elastic scattering data for 500 MeV $\vec{p}+{}^{12,13}C$ are presented. The data are described qualitatively with the microscopic RIA-Dirac-equation model;[18] quantitative fits are obtained with empirical potentials. The measured spin-flip probability does not agree in detail with any of the theoretical predictions shown here or in Ref. 18. However, the D_{NN} data are far from conclusive and more measurements of this quantity are needed, as are continued improvements in the theoretical model. Such improvements might include the use of shell-model wave functions and covariant meson exchange models[28] for the relativistic NN interaction. Sophisticated nonrelativistic scattering models for $p+{}^{13}C$ also need to be developed. Finally, the ${}^{13}C/{}^{12}C$ differential cross section ratio is fit reasonably well with the relativistic DWBA model; this ratio is sensitive to the ${}^{13}C$-${}^{12}C$ structure difference and can be used to constrain the nuclear structure model used in analyses of $\vec{p}+{}^{13}\vec{C}$ elastic scattering data.

This research was supported in part by the U.S. Department of Energy, the Robert A. Welch Foundation, and the National Science Foundation.

---

*Present address: Applied Research Laboratories, University of Texas, Austin, TX 78713.

†Present address: Department of Physics, University of Udine, 33100 Udine, UD, Italy.

[1]G. S. Blanpied et al., Phys. Rev. Lett. **39**, 1447 (1977), and references cited therein.

[2]G. W. Hoffmann et al., Phys. Rev. Lett. **40**, 1256 (1978).

[3]L. Ray, G. W. Hoffmann, G. S. Blanpied, W. R. Coker, and R. P. Liljestrand, Phys. Rev. C **18**, 1756 (1978), and references cited therein.

[4]G. J. Igo et al., Phys. Lett. **81B**, 151 (1979), and references cited therein.

[5]G. W. Hoffmann et al., Phys. Rev. C **21**, 1488 (1980).

[6]G. W. Hoffmann et al., Phys. Rev. C **24**, 541 (1981).

[7]G. W. Hoffmann et al., Phys. Rev. Lett. **47**, 1436 (1981).

[8]A. Rahbar et al., Phys. Rev. Lett. **47**, 1811 (1981).

[9]G. S. Blanpied, B. G. Ritchie, M. L. Barlett, G. W. Hoffmann, J. A. McGill, M. A. Franey, and M. Gazzaly, Phys. Rev. C **32**, 2152 (1985).

[10]B. Aas et al., Nucl. Phys. **A460**, 675 (1986).

[11]R. W. Fergerson et al., Phys. Rev. C **33**, 239 (1986).

[12]G. W. Hoffmann et al., Phys. Rev. C **37**, 1307 (1988).

[13]S. Shim, B. C. Clark, S. Hama, E. D. Cooper, R. L. Mercer, L. Ray, and G. W. Hoffmann, Phys. Rev. C **38**, 1968 (1988).

[14]J. J. Jarmer, S. Penttilä, D. Hill, T. Kasprzyk, M. Krumpole, M. L. Barlett, G. W. Hoffmann, and L. Ray, Nucl. Instrum. Methods A **250**, 576 (1986).

[15]D. Hill, T. Kasprzyk, J. J. Jarmer, S. Penttilä, M. Krumpole, G. W. Hoffmann, and M. Purcell, Nucl. Instrum. Methods A **277**, 319 (1989).

[16]Proceedings of the LAMPF Workshop on Physics with Polarized Nuclear Targets, Los Alamos, 1986, edited by G. Burleson, W. Gibbs, G. Hoffmann, J. J. Jarmer, and N. Tanaka, LAMPF Report No. LA-10772-C, 1986.

[17]LAMPF Proposal 955, Spokesmen: G. W. Hoffmann, R. L. Ray, M. L. Barlett, and J. J. Jarmer.

[18]L. Ray, G. W. Hoffmann, M. L. Barlett, J. D. Lumpe, B. C. Clark, S. Hama, and R. L. Mercer, Phys. Rev. C **37**, 1169 (1988).

[19]J. A. McNeil, J. Shepard, and S. J. Wallace, Phys. Rev. Lett.

50, 1439 (1983); 1443 (1983); B. C. Clark, S. Hama, R. L. Mercer, L. Ray, and B. D. Serot, Phys. Rev. Lett. **50**, 1644 (1983).

[20]L. Ray and G. W. Hoffmann, Phys. Rev. C **31**, 538 (1985).

[21]L. Ray, Phys. Rev. C **19**, 1855 (1979).

[22]J. J. Kelly, Phys. Rev. C **39**, 2120 (1989).

[23]See AIP Document No. PAPS PRVCA-41-1651-17 for a 17 page listing of the data shown here. Order by PAPS number and jornal reference from American Institute of Physics, Physics Auxiliary Publication Service, 335 East 45th Street, New York, N.Y. 10017. The prepaid price is $1.50 for a microfiche, or $5.00 for a photocopy. Airmail additional.

[24]B. C. Clark, in *Medium Energy Nucleon and Antinucleon Scattering,* Vol. 243 of *Lecture Notes in Physics,* edited by H. V. von Geramb (Springer-Verlag, Berlin, 1985), p. 391.

[25]R. A. Arndt, L. D. Roper, R. A. Bryan, R. B. Clark, B. J. VerWest, and P. Signell, Phys. Rev. D **28**, 97 (1983).

[26]I. Sick and J. S. McCarthy, Nucl. Phys. **A150**, 631 (1970).

[27]C. J. Horowitz and B. D. Serot, Nucl. Phys. **A368**, 503 (1981).

[28]N. Ottenstein, S. J. Wallace, and J. A. Tjon, Phys. Rev. C **38**, 2272 (1988); **38**, 2289 (1988).